Unanticipated mechanisms of covalent inhibitor and synthetic ligand cobinding to PPARγ

Jinsai Shang [1,2,*] and Douglas J. Kojetin [1,3,4,5,6,*]

[1] Department of Integrative Structural and Computational Biology, Scripps Research and The Herbert Wertheim UF Scripps Institute for Biomedical Innovation & Technology, Jupiter, Florida, United States
[2] School of Basic Medical Sciences, Guangzhou Laboratory, Guangzhou Medical University, Guangzhou, China.
[3] Department of Biochemistry, Vanderbilt University, Nashville, Tennessee, United States.
[4] Center for Structural Biology, Vanderbilt University, Nashville, Tennessee, United States
[5] Vanderbilt Institute of Chemical Biology, Vanderbilt University, Nashville, Tennessee, United States
[6] Center for Applied AI in Protein Dynamics, Vanderbilt University, Nashville, Tennessee, United States
* Correspondence: shang_jinsai@gzlab.ac.cn (J.S.) and douglas.kojetin@vanderbilt.edu (D.J.K.)

ABSTRACT

Peroxisome proliferator-activated receptor gamma (PPARγ) is a nuclear receptor transcription factor that regulates gene expression programs in response to ligand binding. Endogenous lipids and synthetic ligands, including covalent antagonist inhibitors such as GW9662 and T0070907, are thought to compete for the orthosteric pocket in the ligand-binding domain (LBD). However, we previously showed that synthetic PPARγ ligands can cooperatively cobind with and reposition a bound endogenous orthosteric ligand to an alternate site, synergistically regulating PPARγ structure and function (Shang et al., 2018). Here, we reveal the structural mechanism of cobinding between a synthetic covalent antagonist inhibitor with other synthetic ligands. Biochemical and NMR data show that covalent antagonist inhibitors weaken—but do not prevent—the binding of other synthetic ligands via an allosteric mechanism rather than direct ligand clashing. The covalent ligands shift the LBD ensemble toward a transcriptionally repressive conformation, which structurally clashes with and reduces the orthosteric binding affinity of non-covalent synthetic ligands. Crystal structures reveal different non-covalent synthetic ligand-specific cobinding mechanisms ranging from alternate site binding to unexpectedly adopting an orthosteric binding mode by altering the covalent ligand binding pose. Our findings not only highlight the significant flexibility of the PPARγ orthosteric pocket and its ability to accommodate multiple ligands simultaneously, but also demonstrate that GW9662 and T0070907 should not be used as reliable chemical tools to inhibit the binding of other ligands to PPARγ.

INTRODUCTION

Peroxisome proliferator-activated receptor γ (PPARγ) is a ligand-regulated nuclear receptor transcription factor that regulates gene expression programs controlling adipogenesis and insulin sensitization. Endogenous PPARγ ligands, which include lipids and fatty acids, bind to an orthosteric pocket within the PPARγ ligand-binding domain (LBD) and function as PPARγ agonists that activate gene programs [1–7]. Synthetic small molecule PPARγ ligands, which include FDA-approved antidiabetic drugs, also bind to the same orthosteric pocket, most of which function as agonists that activate PPARγ-mediated transcription. Endogenous and synthetic ligands were originally thought to compete for binding to the PPARγ orthosteric pocket. However, we previously showed that endogenous and synthetic ligands can cobind to PPARγ, likely due to the large size and flexibility of the orthosteric pocket, and synergistically influence PPARγ structure and function [8].

The structural mechanism of agonist-induced activation of PPARγ transcription has been revealed by structural biology studies including NMR spectroscopy and crystal structures. In the absence of ligand, the apo (ligand-free) PPARγ LBD dynamically exchanges between two or more structural conformations [9]. NMR data show that a critical structural element in the LBD called activation function-2 (AF-2) helix (helix 12), which is part of the AF-2 coactivator binding surface, exchanges between active and repressive conformations that can be stabilized upon binding ligand [10]. Agonist binding to the orthosteric pocket stabilizes a solvent exposed helix 12 conformation that enables high affinity binding of coactivators and increases transcription [11,12]. Transcriptionally neutral antagonists and repressive inverse agonists developed from orthosteric agonist ligand scaffolds bind via a similar mechanism of agonists but stabilize non-active helix 12 conformations [13–16].

GW9662 and T0070907 are covalent ligands originally described as antagonists as they bind via a nucleophilic substitution mechanism to Cys285 located within the orthosteric pocket and were shown to inhibit binding of select reference PPARγ agonists [17,18]. These ligands have been used extensively by the field as covalent antagonist inhibitors to block other synthetic ligands from binding PPARγ to test for synthetic ligand specificity in functional experiments. However, we previously showed GW9662 and T0070907 do not block all ligands from binding to PPARγ [8,19–21]—and moreover, they have distinct pharmacological PPARγ functions as a transcriptionally neutral antagonist (GW9662) and repressive inverse agonist (T0070907) [22]. Although these covalent ligands have similar pharmacological functions to orthosteric non-covalent antagonists and inverse agonists, GW9662 and T0070907 function through a different structural mechanism: they slow the rate of exchange between transcriptionally active

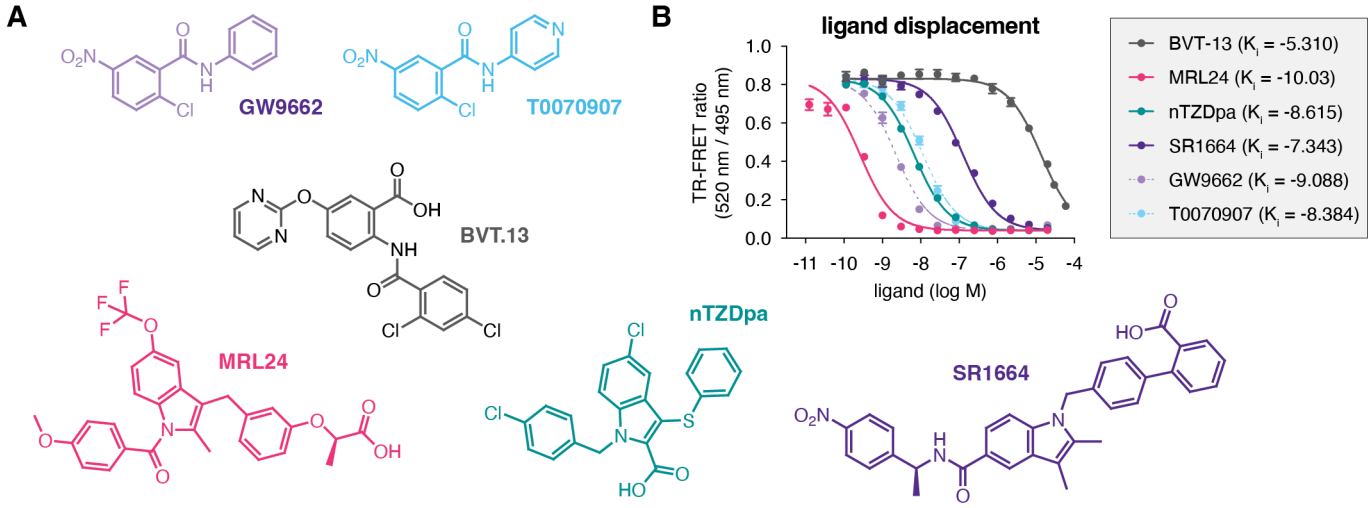

Figure 1. Compounds used in the study and relative affinities in a ligand displacement assay.
(**A**) Chemical structures of the compounds. (**B**) TR-FRET ligand displacement data for the compounds (n=3; mean ± s.d.).

and repressive conformations natively populated in the apo-LBD, with T0070907 having a more pronounced effect than GW9662 [10,23]. In the transcriptionally repressive conformation stabilized by covalent inverse agonists, helix 12 adopts a solvent-occluded conformation within the orthosteric pocket that overlaps with orthosteric ligand binding poses [10,23–25]. These and other published studies have informed a ligand activation model whereby agonist binding to the orthosteric pocket either displaces helix 12 from a solvent occluded repressive conformation within the orthosteric pocket to a solvent exposed active conformation, or selects for an active helix 12 conformation from the dynamic LBD ensemble [26].

What remains unclear is the structural basis of covalent inhibitor and synthetic ligand cobinding. This ligand cobinding mechanism was originally discovered in studies of alternate site ligand binding [19–21,27–30]. Structural studies have mapped the alternate ligand-binding site [19,20] when two equivalents of a synthetic ligand bind, one to the orthosteric pocket and another to the entrance of the orthosteric pocket [26]. NMR and biochemical data revealed non-covalent synthetic compounds can still bind to the PPARγ LBD in the presence of a covalent orthosteric inhibitor [19–21]. While it is presumed that the non-covalent synthetic compound adopts a non-orthosteric binding mode at an alternate site, crystal structures to verify this cobinding mechanism are still needed. Here, using structural biology studies including NMR and crystallography, we confirm that GW9662 and T0070907 do not prevent other synthetic ligands from binding to PPARγ. Furthermore, we demonstrate that certain synthetic ligands can unexpectedly adopt an orthosteric binding pose when cobound with a covalent antagonist inhibitor.

RESULTS

Covalent inhibitor and synthetic ligand cobinding influences PPARγ LBD function

We assembled a set of non-covalent synthetic PPARγ ligands previously shown to bind the PPARγ LBD via two molar equivalents or bind in the presence of a covalent ligand, GW9662 or T0070907 [19] (**Figure 1A**). Using a time-resolved fluorescence resonance energy transfer (TR-FRET) biochemical ligand displacement assay, we verified the ligands bind PPARγ LBD with K_i values (**Figure 1B**) consistent with published data [31–34]. These ligands are generally classified as partial agonists that activate PPARγ transcription with limited or weak efficacy, or non-agonists/antagonists that are transcriptionally neutral.

We profiled the non-covalent synthetic ligands using TR-FRET coregulator peptide interaction assays (**Figure 2**) to determine how the compounds affect interaction between the PPARγ LBD and peptides derived from NCoR1 corepressor and TRAP220/MED1 coactivator proteins, two coregulator proteins that influence PPARγ transcription in cells [35,36]. Consistent with their partial agonist and/or antagonist profiles, the compounds did not significantly increase interaction with the TRAP220 coactivator peptide. Only two compounds, nTZDpa and SR1664, caused notable changes in the coactivator TR-FRET assay. Of these, nTZDpa showed a biphasic transition that may be due to the binding of more than one nTZDpa molecule, which is also suggested by 2D [^{1}H,^{15}N]-TROSY-HSQC NMR data where chemical shift perturbations (CSPs) are observed going from 1 to 2 equivalents of added ligand (**Supplementary Figure S1**).

We next performed TR-FRET coregulator interaction assays using PPARγ LBD protein that was first pretreated with a covalent ligand, GW9662 or T0070907, followed by titration of the non-covalent synthetic ligands. When bound to GW9662 or T0070907, corepressor peptide binding affinity to the LBD is progressively strengthened upon binding to GW9662 and T0070907 while coactivator peptide affinity is weakened according to their neutral and repressive pharmacological activities, respectively [23]. As a result of this change in coregulator affinity, the baseline TR-FRET signal progressively increases in the corepressor assay and decreases in the coactivator assay. Titration of the synthetic ligands shows notable changes in the NCoR1 corepressor TR-FRET assay, where the ligands decrease NCoR1 peptide interaction with IC_{50} profiles with a similar rank-order to ligand K_i values (MRL24 < nTZDpa < SR1664 < BVT.13). Relatively minor changes are observed for the ligands in the TRAP220/MED1 coactivator TR-FRET assay

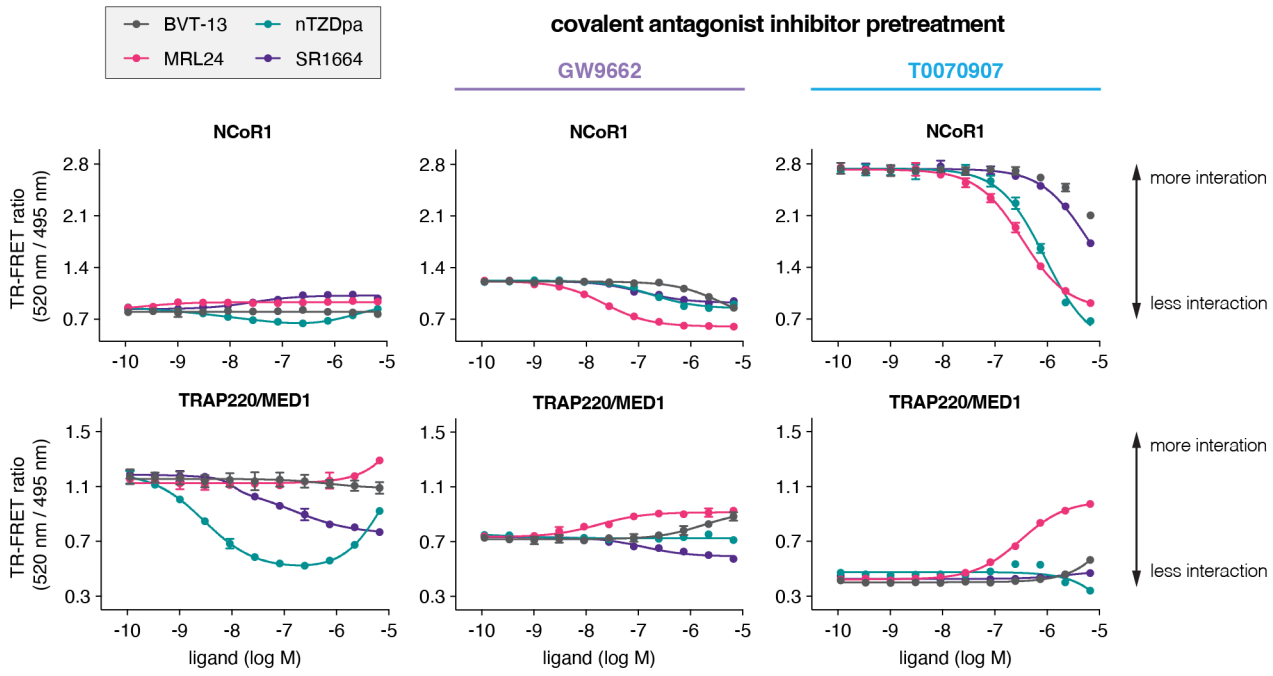

Figure 2. Covalent inhibitor and non-covalent synthetic ligand cobinding functional profiling in TR-FRET coregulator interaction assays. Experiments were performed using PPARγ LBD protein with or without preincubation of GW9662 or T0070907 to determine how the non-covalent synthetic ligands influence recruitment of peptides derived from NCoR1 corepressor protein and TRAP220/MED1 coactivator protein (n=3; mean ± s.d.).

except for MRL24, which shows a concentration-dependent increase in coactivator peptide recruitment. Taken together, these data indicate the functional effect of synthetic ligands binding to PPARγ LBD in the presence of a covalent inhibitor is decreased corepressor peptide interaction. Notably, the synthetic ligand IC_{50} values are weakened (right shifted) more by the inverse agonist T0070907 compared to the neutral antagonist GW9662, suggesting that pharmacological repressive ligand efficacy may be involved in the ligand cobinding inhibitory mechanism.

NMR studies indicate covalent inhibitors allosterically weaken cobinding of non-covalent synthetic ligands by stabilizing a repressive conformation

Two mechanisms may contribute to the covalent inhibitor mechanism of weakening synthetic ligand cobinding. The covalent ligands could structurally overlap or clash with synthetic ligand orthosteric binding modes, leading to alternate site binding with a reduced binding affinity. In this case, the relatively simple phenyl group (GW9662) to pyridyl group (T0070907) change would somehow lead to a more robust clash between the covalent inhibitor and synthetic ligand. Alternatively, the TR-FRET data suggested a different mechanism that involves the repressive efficacy of the covalent ligand. The pharmacological shift from a neutral covalent antagonist (GW9662) to repressive covalent inverse agonist (T0070907) may allosterically shift the dynamic LBD ensemble towards a transcriptionally repressive conformation, where helix 12 adopts a solvent occluded conformation within the orthosteric pocket that structurally clashes with orthosteric binding of a synthetic ligand. In this case, synthetic ligand binding to T0070907-bound PPARγ LBD would significantly influence the NMR-detected repressive LBD conformation where helix 12 is within the orthosteric pocket more than the active LBD conformation where helix 12 is solvent exposed and not occluding the orthosteric pocket.

To structurally assess the non-covalent cobinding mechanism, we performed protein NMR footprinting by comparing 2D [^{1}H,^{15}N]-TROSY-HSQC NMR data of ^{15}N-labeled PPARγ LBD preincubated with a covalent ligand (GW9662 or T0070907) in the absence or presence of a synthetic ligand. Non-covalent ligand cobinding to GW9662-bound LBD shows NMR CSPs for select peaks (**Figure 3A**). In contrast, NMR CSPs are more pronounced for non-covalent ligand binding to T0070907-bound LBD (**Figure 3B**). Focusing on Gly399, a residue near the AF-2 surface that displays two T0070907-bound NMR peaks in slow exchange corresponding to the active or repressive LBD state but only one GW9662-bound active state peak [10,22,23], cobinding of the non-covalent synthetic ligand causes the two NMR peaks in slow exchange to converge to one NMR peak. The NMR peaks corresponding to the repressive T0070907-bound conformation disappear, while the remaining peaks have NMR chemical shift values similar to the T0070907-bound active state but shifted along the active-repressive continuum (i.e., diagonal between the active and repressive T0070907-bound NMR peaks) that correlates with function [23].

Among the synthetic ligands we tested, MRL24 cobinding shows an increase in TRAP220 coactivator peptide recruitment to T0070907-bound PPARγ LBD and the largest shift NMR-detected shift of the LBD conformational ensemble towards an active state. In contrast, nTZDpa cobinding shows an antagonist-like profile

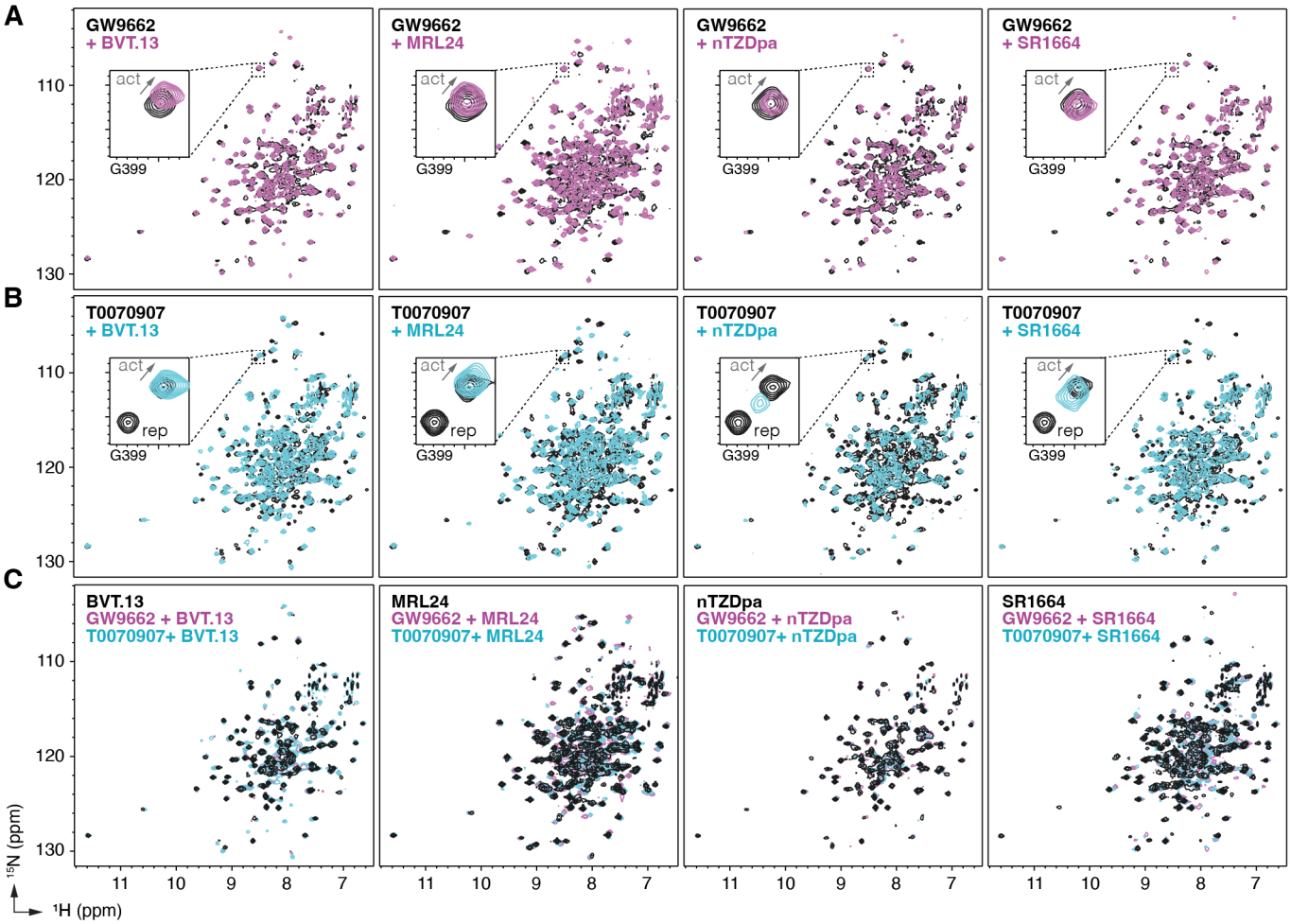

Figure 3. NMR implicates covalent inhibitor-induced stabilization of a repressive LBD conformation in the mechanism of weakening non-covalent synthetic ligand cobinding.
Overlays of 2D [^{1}H,^{15}N]-TROSY-HSQC NMR data of ^{15}N-labeled PPARγ LBD preincubated with covalent inhibitor, (**A**) GW9662 or (**B**) T0070907, in the absence or presence of the indicated non-covalent synthetic ligands added at 2 molar equivalents. (**C**) Overlays of 2D [^{1}H,^{15}N]-TROSY-HSQC NMR data of ^{15}N-labeled PPARγ LBD in the presence of non-covalent synthetic ligands (singly bound state) compared to the cobound states with a covalent inhibitor.

in the TR-FRET data, decreasing both NCoR1 corepressor and to a lesser degree TRAP220 coactivator interaction, and shifts the NMR-detected shift of the LBD conformational ensemble towards an intermediate state between the active and repressive T0070907-observed populations.

Taken together, these NMR-detected observations support the mechanism whereby the repressive conformation helix 12 within the orthosteric pocket of T0070907-bound LBD is displaced to a solvent-exposed active conformation. Furthermore, comparison of 2D [^{1}H,^{15}N]-TROSY-HSQC NMR data of ^{15}N-labeled PPARγ LBD bound to the synthetic ligands alone, or cobound with GW9662 or T0070907, show similar spectral profiles with more subtle CSPs (**Figure 3C**) compared to the larger NMR CSPs observed when comparing ^{15}N-labeled PPARγ LBD bound to each synthetic ligand alone or T0070907-bound LBD relative to GW9662-bound LBD (**Supplementary Figure S2**) [10]. This suggests the active conformation of the PPARγ LBD when bound to a synthetic ligand alone vs. cobound to a covalent ligand are similar, which is supported by the TR-FRET data (**Figure 2**) showing that synthetic ligand cobinding to T0070907-bound PPARγ LBD decreases corepressor peptide interaction.

Crystal structures reveal disparate alternate site ligand binding poses

To visualize the ligand cobinding poses, we first crystalized complexes of PPARγ LBD covalently bound to GW9662 or T0070907, which produced solvent exposed active (chain A) and inactive (chain B) helix 12 conformations similar to apo-PPARγ LBD [37], then we added synthetic ligands to the crystals using soaking methods. We obtained seven crystal structures in total where each synthetic ligand was cobound to either GW9662 or T0070907, except for SR1664 for which we only obtained a structure cobound to T0070907 (**Supplementary Table S1 and Supplementary Figure S3**). In most structures, electron density was observed for non-covalent and covalent ligands in both chains. However, in the nTZDpa structures, the covalent ligand was not observed in chain A; and nTZDpa was observed in chains A and B when cobound to GW9662, but only chain B when cobound to T0070907.

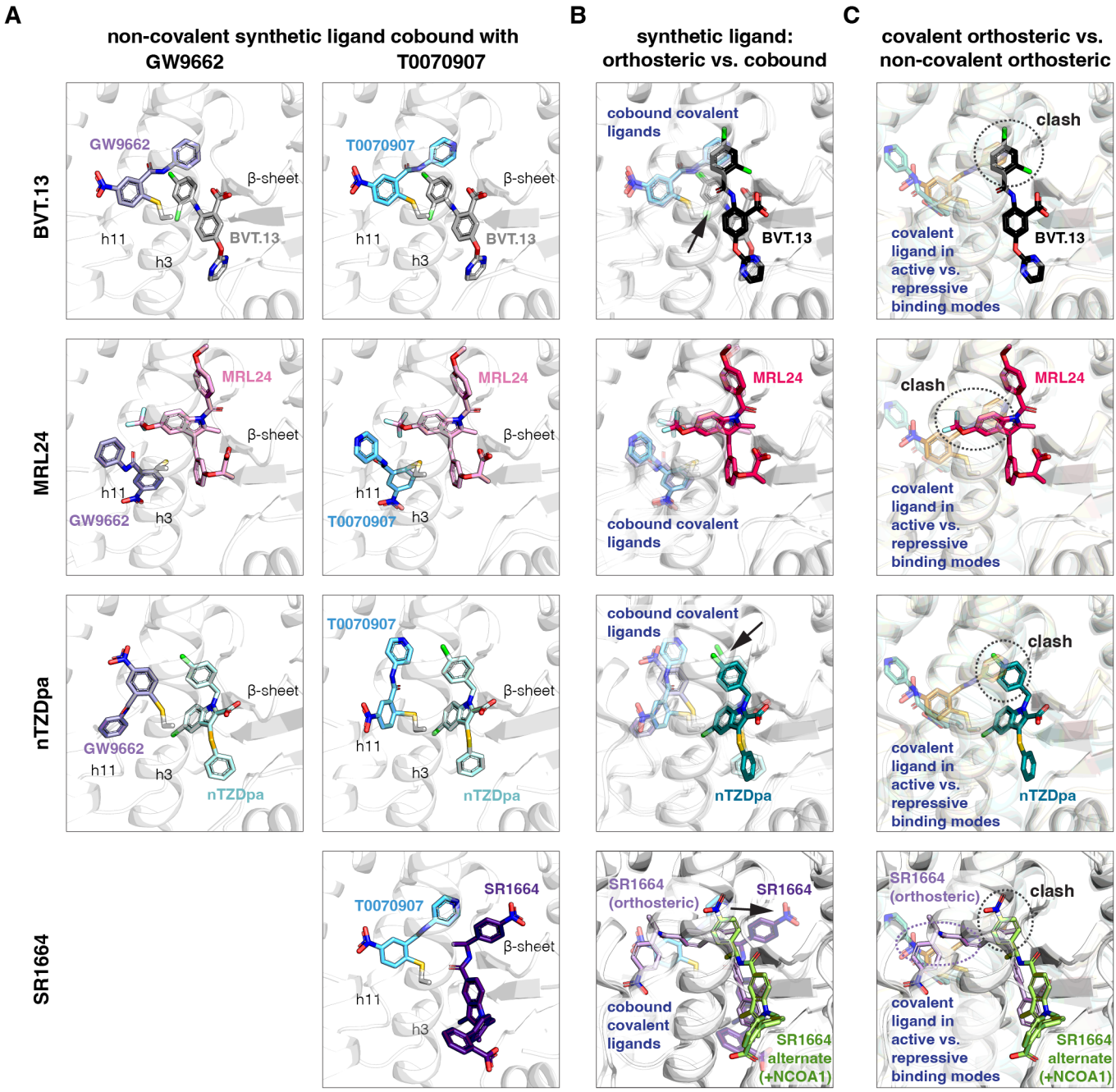

Figure 4. Non-covalent synthetic ligands adopt orthosteric binding modes when cobound with a covalent inhibitor.
(**A**) Ligand cobinding modes in crystal structures of PPARγ LBD. (**B**) Comparison of the non-covalent synthetic ligand orthosteric binding mode (singly bound) and ligand cobinding mode with a covalent inhibitor (transparent sticks). Differences between these binding modes are indicated with a black arrow. (**C**) Structural clashes observed between the covalent inhibitor orthosteric binding mode (transparent sticks) and the non-covalent synthetic ligand binding mode. PDB codes for crystal structures used in the overlays are listed in the Methods section.

We compared our cobound crystal structures to published structures of PPARγ LBD bound to non-covalent ligands—BVT.13 [38], MRL24 [38], nTZDpa [38], and SR1664 alone [16] or cobound to NCOA1 coactivator peptide [39] —and alone to covalent ligands—GW9662 [8] and T0070907 [22]. Overall, the LBD conformations when bound to a single ligand or cobound two ligands are highly similar, with only relatively minor conformational changes in certain residue side chains. Although this is largely influenced by the crystallized forms used for soaking, these findings are also consistent with the aforedescribed 2D NMR data, which indicates a similar LBD conformation for these different liganded states.

Focusing on the non-covalent synthetic ligand cobinding poses (**Figure 4A**), most of the structures surprisingly showed that the ligand adopts a cobound conformation similar to orthosteric binding pose observed in crystals structures of PPARγ LBD bound to the synthetic ligand alone (**Figure 4B**). Slight reorientations of portions of the synthetic ligand occur to accommodate the

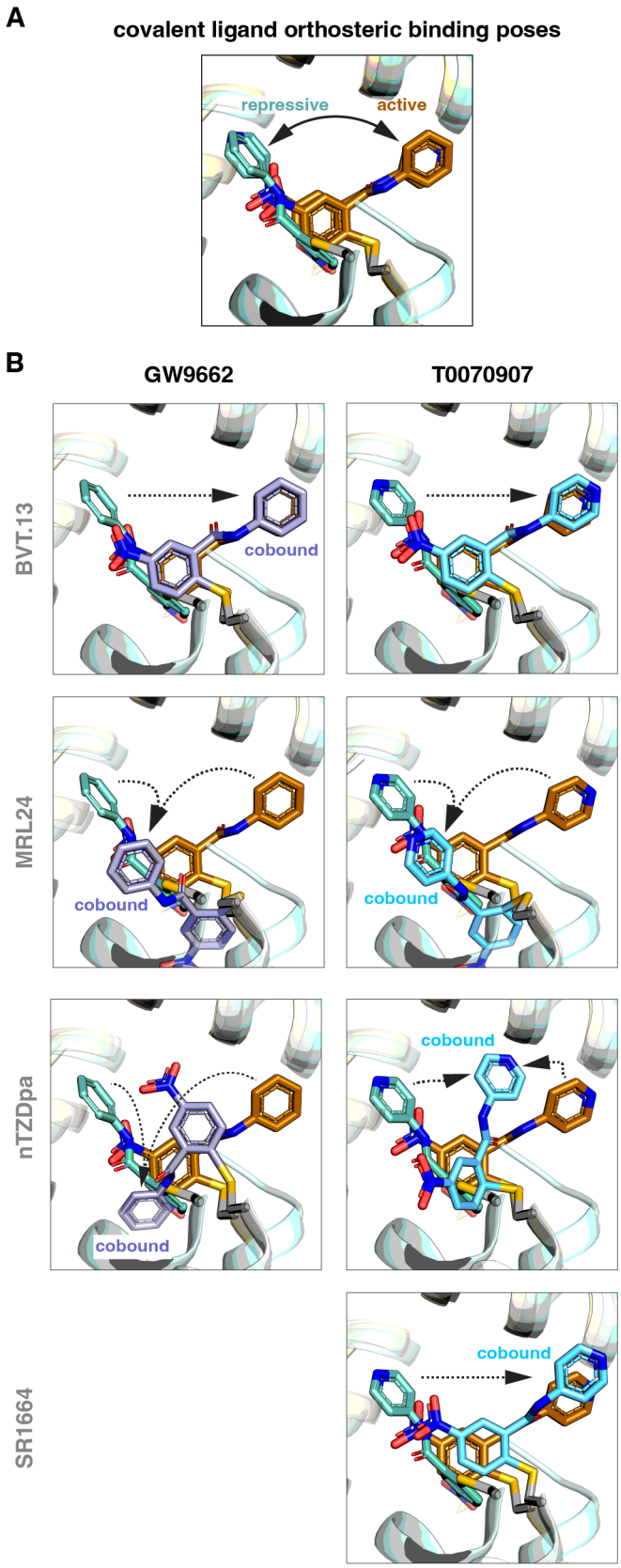

cobinding mode, as there are clashes between the synthetic orthosteric and covalent orthosteric ligand binding modes (**Figure 4C**). Of note, below we use "orthosteric binding pose" to refer to the crystallized ligand conformation when PPARγ LBD is bound to a single ligand.

The BVT.13 cobinding pose is similar to its orthosteric binding pose located near the β-sheet. However, the 2,4-dichloro group clashes with the orthosteric GW9662 and T0070907 binding poses, specifically the phenyl and pyridyl groups respectively, resulting in a slight reorientation of the 2,4-dichloro group to accommodate the cobound state. The MRL24 cobinding pose is also similar to its orthosteric ligand binding pose, which was surprising given its larger scaffold size significantly clashes with the orthosteric covalent ligand binding pose. The nTZDpa cobinding pose is also similar to its orthosteric binding pose near the β-sheet. However, the 1-chloro group clashes with the orthosteric covalent ligand binding pose, resulting in a minor reorientation in the cobinding pose. Finally, the SR1664 cobinding pose reveals an alternate site binding mode similar to the crystallized binding pose in the presence of NCOA1 peptide, with a slight reorientation of the benzoic acid group that avoids a clash with the orthosteric T0070907 binding pose. Notably, these alternate site binding modes are distinct from the orthosteric SR1664 binding mode obtained without coregulator peptide, which shows a large steric clash with the orthosteric covalent ligand binding pose.

Focusing on the covalent ligand binding poses, previously determined crystal structures [10] show that GW9662 and T0070907, when bound alone, are oriented in different directions within the orthosteric pocket in the active state when soaked into apo-PPARγ LBD or repressive state when cobound to NCoR1 corepressor peptide, pointing towards or away from the β-sheet surface, respectively (**Figure 5A**). Cobinding of a non-covalent synthetic ligand has different effects on the covalent ligand binding pose (**Figure 5B**). For BVT.13, the covalent ligand cobinding pose is similar to the orthosteric binding pose. For MRL24, the cobound covalent ligands adopt a similar binding pose that is different from the active and repressive orthosteric binding poses. For nTZDpa, the cobound covalent ligands adopt different orientations, both of which are distinct from the active and repressive covalent ligand only-bound states. For SR1664, the cobinding mode of T0070907 is similar to the orthosteric binding mode. These structures show that the conformation of the covalent ligand can change and adapt to the cobound non-covalent ligand.

Notably, orthosteric ligand K_i values for the non-covalent compounds (**Figure 1B**) correlate with the ability of the non-covalent ligand to push the covalent ligand into a cobinding binding mode that is distinct from the active and repressive covalent ligand binding modes (**Figure 5B**). MRL24 and nTZDa, which are the most potent non-covalent ligands tested, pushed the covalent ligands into different non-natural conformations, whereas BVT.13 and SR1664 do not. Taken together with

Figure 5. Covalent inhibitors adopt different binding modes to accommodate a cobound non-covalent synthetic ligand.
(**A**) Structural overlay showing the orthosteric binding modes of GW9662 and T0070907 in crystal structures of PPARγ LBD in active and repressive conformations. (**B**) Comparison of the covalent binding modes when singly bound (orthosteric) and cobound to a non-covalent synthetic ligand. Black arrows indicate the conformational differences between the orthosteric binding modes vs. cobinding modes. PDB codes for crystal structures used in the overlays are listed in the Methods section.

structural data showing that the covalent ligands naturally exchange between different active and repressive binding poses [10,22], these findings indicate the malleability of the dynamic orthosteric pocket, the natural orthosteric binding mode of the non-covalent ligand, and the relative orthosteric affinity of the non-covalent ligand may determine whether the covalent ligand traps a non-covalent ligand in the entrance to and/or the β-sheet region of the orthosteric pocket.

DISCUSSION

Crystal structures of PPARγ bound to covalent and non-covalent synthetic ligands have shown overlapping ligand binding modes, indicating the covalent ligands should block binding of the non-covalent ligands. We and others have posited that cobinding of a non-covalent synthetic ligand to the PPARγ LBD prebound to a covalent ligand (GW9662 or T0070907) would reveal an alternate site binding mode, different than the crystallized binding modes. To our surprise, the non-covalent ligand can bind via its native orthosteric binding mode by pushing the covalent ligand aside, or slightly adapt its binding mode within the orthosteric pocket. Our structural analysis of non-covalent ligand cobinding with a covalent ligand reveals several important observations and conclusions.

Each of the non-covalent synthetic ligands utilizes unique mechanisms to cobind with the covalent ligands, as inferred from our crystal structures in which pre-formed crystals of the PPARγ LBD were soaked with non-covalent synthetic ligands BVT.13 cobinds to a region of the orthosteric pocket that only slightly overlaps with the orthosteric covalent ligand binding pose, adopting a cobinding pose that is similar to when soaked into apo-PPARγ LBD crystals. MRL24 and nTZDpa cobinding pushes the covalent orthosteric ligand into a different conformation, allowing these ligands to adopt their orthosteric binding modes in the cobound state. This finding was surprising for MRL24 in particular, as its orthosteric binding mode overlaps considerably with the orthosteric covalent ligand binding mode. In contrast, SR1664 cobinding occurs to the so-called alternate site, located at the entrance to the orthosteric pocket.

Our data provide support to structural model where in the absence of ligand, the PPARγ LBD exchanges between a transcriptionally repressive conformation where helix 12 is solvent occluded within the orthosteric pocket and a solvent exposed active conformation [10]. T0070907 binding slows the rate of exchange between these two conformations, stabilizing a long-live active and repressive state [22]. GW9662-bound PPARγ LBD also samples active and repressive states, as observed by PRE NMR [10], though the active conformation is more abundantly populated [40]. Agonist binding occurs via a two-step mechanism involving a fast encounter complex binding step at the entrance to the orthosteric pocket followed by a slow conformational change where the ligand translocates into the orthosteric pocket [26]. Our NMR data here show that non-covalent ligand cobinding to T0070907-bound PPARγ LBD selects for an active conformation, as the repressive conformation NMR peak disappears. This indicates non-covalent ligand cobinding prevents the LBD from adopting a transcriptionally repressive helix 12 conformation within orthosteric pocket, explaining why non-covalent ligand cobinding of MRL24 and other PPARγ agonists with a covalent ligand activates PPARγ transcription [19–21].

Our findings may have profound implications as these GW9662 and T0070907 have been used in many published studies as covalent inhibitors to block ligand binding to PPARγ to test for binding and functional specificity in cells. As of May 2024, more than 1,900 citations referring to "GW9662 or T0070907" are reported in PubMed. Nearly 1,000 of these publications were published in 2015 or later, after the original report that GW9662 and T0070907 are not effective inhibitors of ligand binding [19], yet many in the field continue to use these compounds as covalent inhibitors. Our findings strongly suggest GW9662 and T0070907 should not be used as antagonists to block binding of other synthetic PPARγ ligands. On the other hand, GW9662 and T0070907 display unique pharmacological properties as a transcriptionally neutral antagonist and repressive inverse agonist, respectively [22], and thus it would be appropriate to use these compounds as pharmacological ligands. A newer generation covalent antagonist inhibitor, SR16832, was reported to more completely inhibit alternate site ligand binding of an analog of MRL24 [21] and thus may be a better choice for the field to use as a covalent ligand inhibitor of PPARγ.

MATERIALS AND METHODS

Materials and reagents

All compounds used in this study—GW9662, T0070907, BVT-13, nTZDpa, MRL24, and SR1664—were obtained from commercial sources including Cayman Chemicals, Tocris Bioscience, and Sigma-Aldrich with purity >95%. Peptides of LXXLL-containing motifs from TRAP220/MED1 (residues 638–656; NTKNHPMLMNLLKDNPAQD) and NCoR1 (2256–2278; DPASNLGLEDIIRKALMGSFDDK) with or without a N-terminal FITC label with a six-carbon linker (Ahx) and an amidated C-terminus for stability were synthesized by LifeTein.

Protein expression and purification

Human PPARγ LBD (residues 203–477, isoform 1 numbering) was expressed in *Escherichia coli* BL21(DE3) cells using autoinduction ZY media or M9 minimal media supplemented with NMR isotopes ($^{15}NH_4Cl$) as a Tobacco Etch Virus (TEV)-cleavable N-terminal His-tagged fusion protein using a pET46 Ek/LIC vector (Novagen) and purified using Ni-NTA affinity chromatography and gel filtration chromatography. The purified proteins were concentrated to 10 mg/mL in a buffer consisting of 20 mM potassium phosphate (pH 7.4), 50 mM potassium chloride, 5 mM tris(2-carboxyethyl)phosphine (TCEP), and 0.5 mM ethylenediaminetetraacetic acid (EDTA). Purified protein was verified by SDS-PAGE as >95% pure. For studies using a covalent orthosteric antagonist, PPARγ LBD protein was incubated with at least a ~1.05x excess of GW9662 or T0070907 at 4°C for 24 h to ensure covalent modification to residue C285, then buffer exchanged the sample to remove excess covalent antagonist and DMSO. Complete attachment of the covalent antagonist occurs within 30–60 minutes, as detected using an LTQ XL™ linear Ion trap mass spectrometer with an electrospray ionization source

(Thermo Scientific).

Crystallization and structure determination

For T0070907- and GW9662-bound PPARγ LBD complexes, protein was incubated at a 1:3 protein/ligand molar ratio in PBS overnight. Proteins were buffer exchanged to remove DMSO and concentrated to 10 mg/mL. All crystals were obtained after 3–8 days at 22°C by sitting-drop vapor diffusion against 50 µL of well solution using 96-well format crystallization plates. The crystallization drops contained 1 µL of protein complex sample mixed with apo crystal seeds prepared by PTFE seed bead (Hampton research) and 1 µL of reservoir solution containing 0.1 M MOPS (pH 7.6) and 0.8 M sodium citrate for T0070907 or GW9662-PPARγ LBD complexes; 0.1 M MES (pH 6.5), 0.2 M ammonium sulfate. The non-covalent ligands (BVT.13, MRL24, nTZDpa, SR1664) were soaked into T0070907 or GW9662-PPARγ LBD complex crystals by adding 1.5 µL of compound at a concentration of 2 mM suspended in reservoir solution containing 5% DMSO for 5 days. Data were processed, integrated, and scaled with the programs Mosflm and Scala in CCP4 [41]. The structure was solved by molecular replacement using the program Phaser [42] implemented in the PHENIX package [43] and used previously published PPARγ LBD structure (PDB code: 1PRG/6ONI) [10,37] as the search model. The structure was refined using PHENIX with several cycles of interactive model rebuilding in COOT [44].

NMR spectroscopy

2D [^{1}H,^{15}N]-TROSY HSQC NMR data of 200 µM ^{15}N-labeled PPARγ LBD, pre-incubated with a 2x molar excess of covalent ligand overnight at 4°C, were acquired at 298K on a Bruker 700 MHz NMR instrument equipped with a QCI cryoprobe in NMR buffer (50 mM potassium phosphate, 20 mM potassium chloride, 1 mM TCEP, pH 7.4, 10% D_2O). Data were processed and analyzed using Topspin 3.0 (Bruker Biospin) and NMRViewJ (OneMoon Scientific, Inc.) [45], respectively. NMR chemical shift assignments previously transferred from rosiglitazone-bound PPARγ LBD [11] to T0070907- and GW9662-bound states [10,22] were used in this study for well-resolved residues with conversed NMR peak positions to the previous ligand-bound forms using the minimum chemical shift perturbation procedure [46].

Time-resolved fluorescence resonance energy transfer (TR-FRET) assay

The time-resolved fluorescence resonance energy transfer (TR-FRET) assays were performed in black 384-well plates (Greiner) with 23 µL final well volume containing 4 nM His_6-PPARγ LBD with or without covalently modification by GW9662 or T0070907, 1 nM LanthaScreen Elite Tb-anti-His Antibody (ThermoFisher), and 400 TRAP220 or NCoR peptide in TR-FRET buffer (20 mM KPO_4 pH 7.4, 50 mM KCl, 5 mM TCEP, 0.005% Tween 20). Compound stocks were prepared via serial dilution in DMSO, added to wells in triplicate, and plates were read using BioTek Synergy Neo multimode plate reader after incubating at 25°C for 1 h. The Tb donor was excited at 340 nm, its emission was measured at 495 nm, and the acceptor FITC emission was measured at 520 nm. Data were plotted using GraphPad Prism as TR-FRET ratio 520 nm/495 nm vs. ligand concentration and fit to sigmoidal dose-response curve equation.

Structural comparisons to published crystal structures

Structural overlays were compared to crystals structures of PPARγ LBD bound to GW9662 (PDB 3B0R), T0070907 (PDB 6C1I) [22], GW9662 and NCoR1 peptide (PDB 8FHE) [23], T0070907 and NCoR1 peptide (6ONI) [10], BVT.13 (PDB 2Q6S) [38], MRL24 (PDB 2Q5P) [38], nTZDpa (PDB 2Q5S) [38], SR1664 and NCOA1 peptide (PDB 5DWL) [39], and SR1664 (PDB 4R2U) [16].

ACKNOWLEDGMENTS

This work was supported in part by the National Institutes of Health (NIH) grant R01DK124870 from the National Institute of Diabetes and Digestive and Kidney Diseases (NIDDK). Use of the Stanford Synchrotron Radiation Lightsource, SLAC National Accelerator Laboratory, is supported by the U.S. Department of Energy, Office of Science, Office of Basic Energy Sciences under Contract No. DE-AC02-76SF00515. The SSRL Structural Molecular Biology Program is supported by the DOE Office of Biological and Environmental Research and by the NIH National Institute of General Medical Sciences (NIGMS) grant P30GM133894. The contents of this publication are solely the responsibility of the authors and do not necessarily represent the official views of NIDDK, NIGMS, NIH, or DOE.

DATA AVAILABILITY

Crystal structures generated during the current study are available in the Protein Data Bank (PDB) under accession codes 8ZFN, 8ZFO, 8ZFP, 8ZFQ, 8ZFR, 8ZFS, 8ZFT as detailed in **Supplementary Table S1**. All other datasets generated and/or analyzed during the current study are available from the corresponding author on reasonable request.

AUTHOR CONTRIBUTIONS

J.S. performed the research. D.J.K. supervised the research. J.S. and D.J.K. conceived and designed the research, analyzed data, and wrote the manuscript.

REFERENCES

1. Itoh, T. *et al.* Structural basis for the activation of PPARgamma by oxidized fatty acids. *Nat. Struct. Mol. Biol.* **15**, 924–931 (2008).
2. Li, Y. *et al.* Molecular recognition of nitrated fatty acids by PPAR gamma. *Nat. Struct. Mol. Biol.* **15**, 865–867 (2008).
3. Malapaka, R. R. V. *et al.* Identification and mechanism of 10-carbon fatty acid as modulating ligand of peroxisome proliferator-activated receptors. *J. Biol. Chem.* **287**, 183–195 (2012).
4. Schopfer, F. J. *et al.* Nitrolinoleic acid: an endogenous peroxisome proliferator-activated receptor gamma ligand. *Proc. Natl. Acad. Sci. U. S. A.* **102**, 2340–2345 (2005).
5. Kliewer, S. A. *et al.* Fatty acids and eicosanoids regulate gene expression through direct interactions with peroxisome proliferator-activated receptors alpha and gamma. *Proc. Natl. Acad. Sci. U. S. A.* **94**, 4318–4323 (1997).
6. Kliewer, S. A. *et al.* A prostaglandin J2 metabolite binds

peroxisome proliferator-activated receptor gamma and promotes adipocyte differentiation. *Cell* **83**, 813–819 (1995).

7. Waku, T. *et al.* Structural insight into PPARgamma activation through covalent modification with endogenous fatty acids. *J. Mol. Biol.* **385**, 188–199 (2009).

8. Shang, J. *et al.* Cooperative cobinding of synthetic and natural ligands to the nuclear receptor PPARγ. *Elife* **7**, e43320 (2018).

9. Johnson, B. A. *et al.* Ligand-induced stabilization of PPARgamma monitored by NMR spectroscopy: implications for nuclear receptor activation. *J. Mol. Biol.* **298**, 187–194 (2000).

10. Shang, J. *et al.* A molecular switch regulating transcriptional repression and activation of PPARγ. *Nat. Commun.* **11**, 956 (2020).

11. Hughes, T. S. *et al.* Ligand and receptor dynamics contribute to the mechanism of graded PPARγ agonism. *Structure* **20**, 139–150 (2012).

12. Shang, J., Brust, R., Griffin, P. R., Kamenecka, T. M. & Kojetin, D. J. Quantitative structural assessment of graded receptor agonism. *Proc. Natl. Acad. Sci. U. S. A.* **116**, 22179–22188 (2019).

13. Frkic, R. L. *et al.* PPARγ Corepression Involves Alternate Ligand Conformation and Inflation of H12 Ensembles. *ACS Chem. Biol.* **18**, 1115–1123 (2023).

14. Frkic, R. L. *et al.* PPARγ in Complex with an Antagonist and Inverse Agonist: a Tumble and Trap Mechanism of the Activation Helix. *iScience* **5**, 69–79 (2018).

15. Zheng, J. *et al.* Chemical Crosslinking Mass Spectrometry Reveals the Conformational Landscape of the Activation Helix of PPARγ; a Model for Ligand-Dependent Antagonism. *Structure* **26**, 1431–1439.e6 (2018).

16. Marciano, D. P. *et al.* Pharmacological repression of PPARγ promotes osteogenesis. *Nat. Commun.* **6**, 7443 (2015).

17. Lee, G. *et al.* T0070907, a selective ligand for peroxisome proliferator-activated receptor gamma, functions as an antagonist of biochemical and cellular activities. *J. Biol. Chem.* **277**, 19649–19657 (2002).

18. Leesnitzer, L. M. *et al.* Functional consequences of cysteine modification in the ligand binding sites of peroxisome proliferator activated receptors by GW9662. *Biochemistry* **41**, 6640–6650 (2002).

19. Hughes, T. S. *et al.* An alternate binding site for PPARγ ligands. *Nat. Commun.* **5**, 3571 (2014).

20. Hughes, T. S. *et al.* Probing the Complex Binding Modes of the PPARγ Partial Agonist 2-Chloro-N-(3-chloro-4-((5-chlorobenzo[d]thiazol-2-yl)thio)phenyl)-4-(trifluoromethyl) benzenesulfonamide (T2384) to Orthosteric and Allosteric Sites with NMR Spectroscopy. *J. Med. Chem.* **59**, 10335–10341 (2016).

21. Brust, R. *et al.* Modification of the Orthosteric PPARγ Covalent Antagonist Scaffold Yields an Improved Dual-Site Allosteric Inhibitor. *ACS Chem. Biol.* **12**, 969–978 (2017).

22. Brust, R. *et al.* A structural mechanism for directing corepressor-selective inverse agonism of PPARγ. *Nat. Commun.* **9**, 4687 (2018).

23. MacTavish, B. *et al.* Ligand efficacy shifts a nuclear receptor conformational ensemble between transcriptionally active and repressive states. *bioRxiv* 2024.04.23.590805 (2024) doi:10.1101/2024.04.23.590805.

24. Irwin, S. *et al.* Biochemical and structural basis for the pharmacological inhibition of nuclear hormone receptor PPARγ by inverse agonists. *J. Biol. Chem.* **298**, 102539 (2022).

25. Orsi, D. L. *et al.* Discovery and Structure-Based Design of Potent Covalent PPARγ Inverse-Agonists BAY-4931 and BAY-0069. *J. Med. Chem.* **65**, 14843–14863 (2022).

26. Shang, J. & Kojetin, D. J. Structural mechanism underlying ligand binding and activation of PPARγ. *Structure* **29**, 940–950.e4 (2021).

27. Arifi, S. *et al.* Targeting the Alternative Vitamin E Metabolite Binding Site Enables Noncanonical PPARγ Modulation. *J. Am. Chem. Soc.* **145**, 14802–14810 (2023).

28. Jang, J. Y. *et al.* Structural basis for differential activities of enantiomeric PPARγ agonists: Binding of S35 to the alternate site. *Biochim. Biophys. Acta: Proteins Proteomics* **1865**, 674–681 (2017).

29. Laghezza, A. *et al.* Identification of the First PPARα/γ Dual Agonist Able To Bind to Canonical and Alternative Sites of PPARγ and To Inhibit Its Cdk5-Mediated Phosphorylation. *J. Med. Chem.* **61**, 8282–8298 (2018).

30. Leijten-van de Gevel, I. A. *et al.* Indazole MRL-871 interacts with PPARγ via a binding mode that induces partial agonism. *Bioorg. Med. Chem.* **68**, 116877 (2022).

31. Choi, J. H. *et al.* Antidiabetic actions of a non-agonist PPARγ ligand blocking Cdk5-mediated phosphorylation. *Nature* **477**, 477–481 (2011).

32. Berger, J. P. *et al.* Distinct properties and advantages of a novel peroxisome proliferator-activated protein [gamma] selective modulator. *Mol. Endocrinol.* **17**, 662–676 (2003).

33. Ostberg, T. *et al.* A new class of peroxisome proliferator-activated receptor agonists with a novel binding epitope shows antidiabetic effects. *J. Biol. Chem.* **279**, 41124–41130 (2004).

34. Acton, J. J., 3rd *et al.* Benzoyl 2-methyl indoles as selective PPARgamma modulators. *Bioorg. Med. Chem. Lett.* **15**, 357–362 (2005).

35. Ge, K. *et al.* Transcription coactivator TRAP220 is required for PPAR gamma 2-stimulated adipogenesis. *Nature* **417**, 563–567 (2002).

36. Yu, C. *et al.* The nuclear receptor corepressors NCoR and SMRT decrease peroxisome proliferator-activated receptor gamma transcriptional activity and repress 3T3-L1 adipogenesis. *J. Biol. Chem.* **280**, 13600–13605 (2005).

37. Nolte, R. T. *et al.* Ligand binding and co-activator assembly of the peroxisome proliferator-activated receptor-gamma. *Nature* **395**, 137–143 (1998).

38. Bruning, J. B. *et al.* Partial agonists activate PPARgamma using a helix 12 independent mechanism. *Structure* **15**, 1258–1271 (2007).

39. Bae, H. *et al.* Mechanistic elucidation guided by covalent inhibitors for the development of anti-diabetic PPARγ ligands. *Chem. Sci.* **7**, 5523–5529 (2016).

40. Chrisman, I. M. *et al.* Defining a conformational ensemble that directs activation of PPARγ. *Nat. Commun.* **9**, 1794 (2018).

41. Agirre, J. *et al.* The CCP4 suite: integrative software for macromolecular crystallography. *Acta Crystallogr D Struct Biol* **79**, 449–461 (2023).

42. McCoy, A. J. *et al.* Phaser crystallographic software. *J. Appl. Crystallogr.* **40**, 658–674 (2007).

43. Adams, P. D. *et al.* PHENIX: a comprehensive Python-based system for macromolecular structure solution. *Acta Crystallogr. D Biol. Crystallogr.* **66**, 213–221 (2010).

44. Emsley, P. & Cowtan, K. Coot: model-building tools for molecular graphics. *Acta Crystallogr. D Biol. Crystallogr.* **60**, 2126–2132 (2004).

45. Johnson, B. A. From Raw Data to Protein Backbone Chemical Shifts Using NMRFx Processing and NMRViewJ Analysis. *Methods Mol. Biol.* **1688**, 257–310 (2018).

46. Williamson, M. P. Using chemical shift perturbation to characterise ligand binding. *Prog. Nucl. Magn. Reson. Spectrosc.* **73**, 1–16 (2013).